



Solvent and electrolyte effects in enhancing the identification of intramolecular electronic communication in a multi redox-active diruthenium tetraferrocenoate complex, a triple-sandwiched dicadmium phthalocyanine and a ruthenocene-containing β -diketone

Henno J. Gericke^a, Nicola I. Barnard^a, Elizabeth Erasmus^a, Jannie C. Swarts^{a,*}, Michael J. Cook^b, Manuel A.S. Aquino^c

^aDepartment of Chemistry, University of the Free State, Bloemfontein 9300, South Africa

^bSchool of Chemical and Biological Sciences, University of East Anglia, Norwich NR4 7TJ, UK

^cSt. Francis Xavier University, Antigonish, Nova Scotia, Canada B2G 2W5

ARTICLE INFO

Article history:

Received 14 December 2009

Received in revised form 3 March 2010

Accepted 11 March 2010

Available online 16 March 2010

Dedicated to Professor W. E. (Bill) Geiger of Vermont for his contributions to the field of electrochemistry.

Keywords:

Ferrocene
Ruthenocene
 β -Diketone
Cadmium
Phthalocyanine
Electrochemistry

ABSTRACT

Enhanced electrochemical resolution of anodic processes is possible in the presence of $[\text{N}(\text{tBu})_4][\text{B}(\text{C}_6\text{F}_5)_4]$, **1**, as supporting electrolyte over that obtained in the presence of $[\text{N}(\text{tBu})_4][\text{PF}_6]$. By changing the anion of the supporting electrolyte to a salt having $[\text{B}(\text{C}_6\text{F}_5)_4]^-$ anions, electrochemical processes of especially cationic analytes can benefit. Thus, the redox chemistry of 0.5 mmol dm⁻³ solutions of $[\text{Ru}_2(\mu\text{-FcCOO})_4(\text{CH}_3\text{CH}_2\text{OH})_2][\text{PF}_6]$, **2**, Fc = ferrocenyl, in $\text{CH}_2\text{Cl}_2/[\text{N}(\text{tBu})_4][\text{B}(\text{C}_6\text{F}_5)_4]$ were found to involve four well-resolved ferrocenyl-based electrochemical reversible redox processes as well as reduction of $\text{Ru}^{\text{III}}-\text{Ru}^{\text{II}}$. At 1.0 mmol dm⁻³ concentrations of **2**, or in the presence of $[\text{N}(\text{tBu})_4][\text{PF}_6]$, the four ferrocenyl processes coalesced into only two waves as a result of $(\text{Fc}^+) \cdots (\text{PF}_6^-)$ ion pairing. Seventeen of the possible 18 one-electron transfer processes of the biscadmium trisphthalocyaninato complex $[\text{Cd}_2[\text{Pc}(\text{C}_6\text{H}_{13})_8]_3]$, **3**, could be observed in $\text{THF}/[\text{N}(\text{tBu})_4][\text{B}(\text{C}_6\text{F}_5)_4]$, but the electrochemical window of $\text{CH}_2\text{Cl}_2/[\text{N}(\text{tBu})_4][\text{B}(\text{C}_6\text{F}_5)_4]$ only allowed detection of 15 of these processes. Although reduction processes were unaffected, THF solvation leading to species such as $(\text{3}^{\text{III}})(\text{THF})_x$ with $1 \leq n \leq 4$ and $x \geq 1$ as well as ion pair formation of the type $(\text{3}^{\text{III}}) \cdots (\text{PF}_6^-)$ prevented good resolution of oxidation processes. The $\text{CH}_2\text{Cl}_2/[\text{N}(\text{tBu})_4][\text{B}(\text{C}_6\text{F}_5)_4]$ system also allowed detection of reversible one-electron transfer ferrocenyl (Fc/Fc⁺) and ruthenocenyl-based (Rc/Rc⁺) processes for both enol and keto isomers of the β -diketone FcC(OCH₂CORc), **4**, Rc = ruthenocenyl. In $\text{CH}_3\text{CN}/[\text{N}(\text{tBu})_4][\text{PF}_6]$, the ruthenocenyl moiety was oxidised to a Ru^{IV} species.

© 2010 Elsevier B.V. All rights reserved.

1. Introduction

Cyclic voltammetry (CV) is possibly the simplest and most versatile electroanalytical technique for the study of electroactive species. The effectiveness of CV having a triangular voltage input signal (i.e. a triangular voltage vs. time plot, see [Supplementary material](#)) is its ability to probe the redox behaviour of an electroactive species at different scan rates (though much faster scan rates are possible, convenient scan rates are between 50 and 500 mV s⁻¹) over a wide potential range using simple equipment [1]. Osteryoung square wave voltammetry (OYSW) utilises a pulsed voltage input signal in step form [2]. Currents are measured at various times during the lifetime of these pulses. From OYSW

voltammetry, better resolution is possible in cases where CV data does not clearly distinguish between poorly resolved (i.e. near-overlapping) multiple redox waves [3]. It is important to recognise, though, that the electrode potentials of closely spaced redox events are notoriously difficult to assess using CV methods. Taube discussed this in detail [3a]. In linear sweep voltammetry (LSV), the dc potential applied to the cell increases linearly very slowly as a function of time (2 mV s⁻¹ maximum compared to 50 mV or faster for CV, depending on active electrode area). From an analytical point of view the LSV type of voltammogram is advantageous because it can be used to accurately determine the relative number of electrons that flow in a particular electrochemical process compared to other electrochemical processes that take place within the same molecule (i.e. the equivalent of integration in NMR) [3].

The formal reduction potential, E° , and a measure of electrochemical reversibility or the amount of electrons (n) that flows per molecule during any single redox process can conveniently

* Corresponding author. Tel.: +27 (0)51 4012781; fax: +27 (0)51 4446384.
E-mail address: swartsjc@ufs.ac.za (J.C. Swarts).

be obtained from Eqs. (1)–(4). By electrochemical reversibility it is meant that the rate of electron transfer between the electrode and substrate is fast enough to maintain the concentration of the oxidised and reduced species in equilibrium, according to the Nernst equation, at the electrode surface at the particular scan rate. In contrast, chemical reversibility implies a compound can both be quantitatively oxidised, and the product can again be quantitatively reduced back to the original material, but there is no limitation on how fast this must happen. An electrochemically reversible couple which is not followed by any chemical reaction should obey Eq. (3) (or its reciprocal – the current ratio of Eq. (3) should be taken as the current of the *reverse* scan divided by the current of the *forward* scan). An electrochemical process that obeys Eq. (3) must inevitably also be chemical reversible, but one that does not obey Eq. (3) can still be chemical reversible, even though it is not any more electrochemically reversible. From the Randles–Sevcik equation (Eq. (4) at 25 °C, [1,4]), peak current measurements of electro-

chemically reversible systems are related to diffusion coefficients, D . If the relationship between i_p and the square root of scan rate (ν in V s^{-1}) is linear, then the electroactive species is in solution rather than surface bound. The diagnostic $\Delta E = 59 \text{ mV}$ for electrochemical reversible one-electron transfer processes are often difficult to achieve without instrument compensation for cell resistance and over potentials. Thus, frequently ΔE values of up to 90 mV for perfectly electrochemically reversible processes are obtained. In these cases, a linear relationship between i_p and $\nu^{1/2}$ is more convenient in demonstrating electrochemical reversibility than ΔE values [5].

$$E^{or} = (E_{pa} + E_{pc})/2 \quad (1)$$

$$\Delta E_p = E_{pa} - E_{pc} = 59/n \text{ mV} \quad (2)$$

$$i_{pc}/i_{pa} = 1 \text{ (denominator is always from the "forward" scan)} \quad (3)$$

$$i_p = (2.69 \times 10^5)n^{3/2}AD^{1/2}\nu^{1/2}C \quad (4)$$

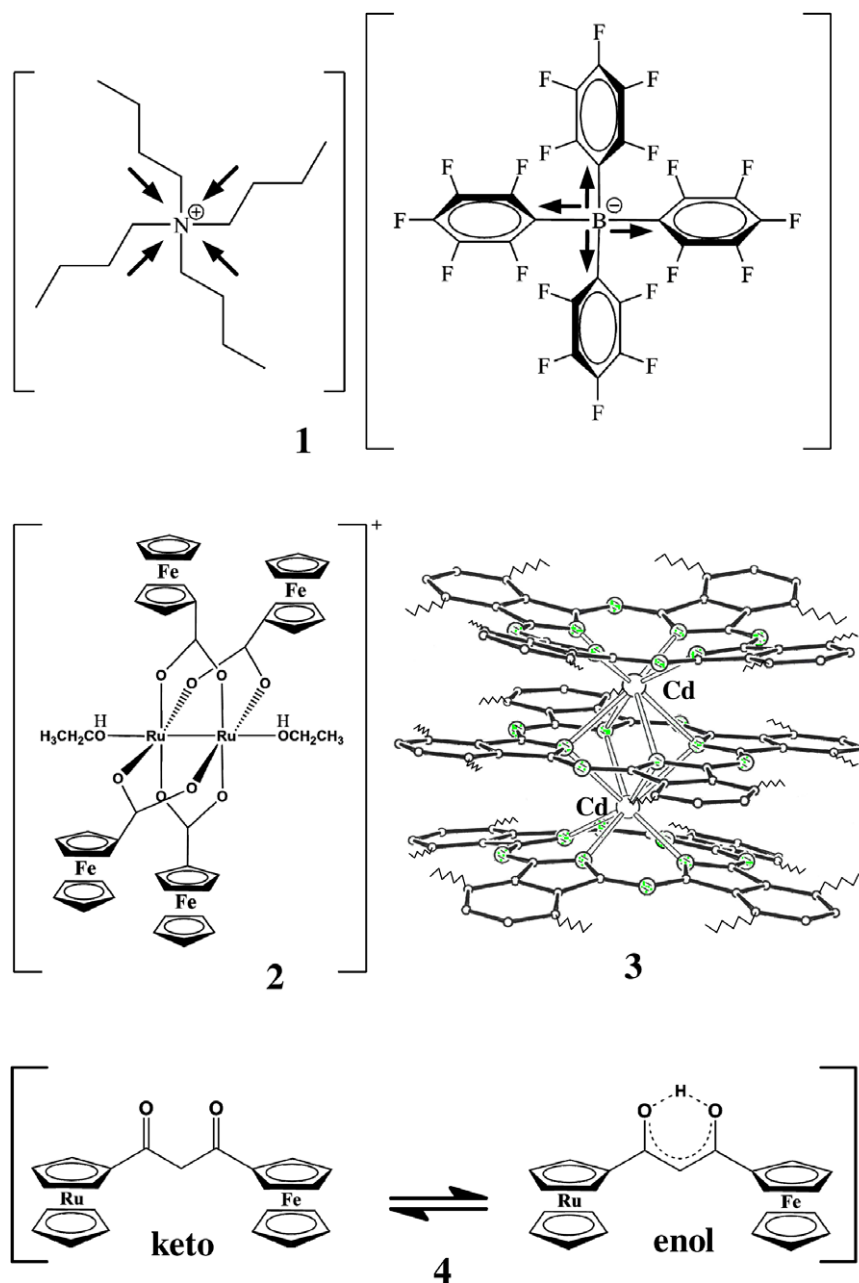


Fig. 1. Structure of the electrolyte $[\text{N}(\text{tBu})_4][\text{B}(\text{C}_6\text{F}_5)_4]$, **1**, as well as complexes **2–4**. Green balls = N from the structure of **3** which has been reported elsewhere [15a]. The arrows in **1** indicate how the electron-donating effect of the butyl groups and the electron withdrawing effect of the C_6F_5 groups dissipate the charges on the N and B atoms.

It is also important to note that E° should not be affected by differences in scan rate in electrochemical reversible processes (it should remain constant). Accurate results from Eqs. (1)–(4) rely on measurements of CV data that are independent of analyte-solvent and analyte-supporting electrolyte interactions. Frequently poor experimental conditions or cell imperfections such as too little supporting electrolyte, solvent and/or supporting electrolyte association with analytes, low solvent dielectric constants, junction potentials, imperfect or dirty electrode surfaces and electrode over-potentials distort peak potential and peak current measurements and lead to inaccurate determinations of many of the above-mentioned data and conclusions that can be drawn from them, including large scatterings in measured diffusion coefficients [6]. Consequently the choice of solvent, supporting electrolyte and reference electrodes are crucial for reliable results.

Traditionally, for non-aqueous experimentation, DMSO or CH_3CN and $[\text{N}^{\text{tBu}}_4][\text{PF}_6]$ or $[\text{ClO}_4]^-$ are favourite solvents and supporting electrolytes. However, both CH_3CN and DMSO frequently co-ordinate to metal complexes to form totally new species [7], and the PF_6^- or ClO_4^- anions frequently form ion-pairs with oxidised species. Due to the explosive nature of the ClO_4^- salts, use of perchlorate-containing supporting electrolytes is strongly discouraged. Ion pair formation, especially with positively charged oxidised species, can be minimised if the negative charge of the anion of the supporting electrolyte can be spread over a large volume, just as the positive charge on the N atom of the $\text{N}^{\text{tBu}}_4^+$ cation are inductively minimised by the four electron-donating butyl groups. Towards supporting electrolytes with limited ion pairing capabilities, the electrolyte $[\text{N}^{\text{tBu}}_4][\text{B}(\text{C}_6\text{F}_5)_4]$, **1**, Fig. 1, and $[\text{N}^{\text{tBu}}_4][\text{B}(\text{C}_6\text{H}_3(\text{CF}_3)_2)_4]$ has been developed by Geiger and Mann, respectively, with very good effect [8]. The $[\text{B}(\text{C}_6\text{F}_5)_4]^-$ anion has an approximate spherical diameter of 10 Å compared to PF_6^- 's diameter of ca. 3.3 Å and therefore will have a lower charge density than PF_6^- .

To minimise solvent-analyte interactions, CH_2Cl_2 is gaining favour over CH_3CN as solvent. However, if a need for solvent with a larger potential window than CH_2Cl_2 exists to study analytes under strong reducing conditions (i.e. more negative potentials), THF may prove to be a beneficial solvent. While THF is nucleophilic and would interact with electrophilic or positively charged species under oxidising conditions, it can be considered non-interactive towards negatively charged (reduced) species.

Because measured potentials vs. a convenient reference electrode such as Ag/Ag^+ (as a silver wire immersed in a 0.01 mol dm^{-3} AgNO_3 solution), or a pseudo reference electrode such as a Ag of Cu wire drift from solvent to solvent or sometimes even from experiment to experiment as conditions such as temperature, cell geometry or concentrations of analytes and supporting electrolytes differ, IUPAC has issued a directive [9] that all electrochemical data be reported vs. an internal standard as first suggested by Gagne et al. [10]. A convenient internal standard is ferrocene or decamethylferrocene [11].

In this communication we practically apply and demonstrate all of the above fundamental aspects by discussing the well-resolved enhanced voltammograms that can be obtained from a voltammetric study of $[\text{Ru}_2(\mu\text{-FcCO})_4(\text{CH}_3\text{CH}_2\text{OH})_2][\text{PF}_6]$, **2**, the biscadmium trisphthalocyaninato complex **3**, and the mixed-metallocene β -diketone $\text{Fc-CO-CH}_2\text{-CO-Rc}$, **4**, where Fc = ferrocenyl, Rc = ruthenocenyl, in $\text{CH}_2\text{Cl}_2/[\text{N}^{\text{tBu}}_4][\text{B}(\text{C}_6\text{F}_5)_4]$. Electrochemical results obtained in the solvents THF, CH_2Cl_2 and CH_3CN are compared.

The electrochemistry of complex **2** was initially reported utilising only $[\text{N}^{\text{tBu}}_4][\text{PF}_6]$ as supporting electrolyte [12], which led to poor resolution of the ferrocenyl peaks. The antineoplastic activity of **2** has also been studied and related to the initial electrochemical results [12a]. The detailed electrochemistry of complex **3** described

before did not describe the advantage of $[\text{N}^{\text{tBu}}_4][\text{B}(\text{C}_6\text{F}_5)_4]$ over $[\text{N}^{\text{tBu}}_4][\text{PF}_6]$ as supporting electrolyte [13]. The isomerisation kinetics of **4** has recently been studied by us in comparison with other β -diketones of the type $\text{Rc-CO-CH}_2\text{-CO-R}$ by spectroscopic and electrochemical means [14]. However, within the context of this publication, **4** serves especially well to demonstrate how the use of both CH_3CN and $[\text{N}^{\text{tBu}}_4][\text{PF}_6]$ results in the generation of a Ru^{IV} product in an electrochemical irreversible process, while in $\text{CH}_2\text{Cl}_2/[\text{N}^{\text{tBu}}_4][\text{B}(\text{C}_6\text{F}_5)_4]$, a reversible $\text{Ru}^{\text{III}}/\text{Ru}^{\text{II}}$ couple followed by a chemical dimerisation process involving Ru^{III} centres is observed.

2. Experimental

2.1. Materials and apparatus

Lithium tetrakis[pentafluorophenyl]borate etherate (Boulder Scientific Corporation, USA), ruthenocene, ferrocene (Strem), aluminium trichloride and other solid reagents (Aldrich) were used without further purification. Dichloromethane and acetonitrile were dried by refluxing under nitrogen over calcium hydride, tetrahydrofuran was dried over Na wire and redistilled just prior to use. Water was double distilled. Complexes **2** [12] and **3** [15] were synthesised as described before. ^1H NMR spectra at 20 °C were recorded on a Bruker Avance DPX 300 NMR spectrometer at 300 MHz with chemical shifts presented as δ values referenced to SiMe_4 at 0.00 ppm utilising acid free CDCl_3 as solvent. Melting points were determined with a Reichert Thermopan microscope with a Kofler hot-stage and are uncorrected. CDCl_3 was made acid free by passing it through basic alumina immediately before use. Elemental analysis was conducted by the Canadian Microanalytical Service, Ltd.

2.2. Syntheses

2.2.1. Synthesis of **1**

An adaption of a published procedure [16] was followed. Solvents used in this synthesis were of the best quality available. Lithium tetrakis[pentafluorophenyl]borate etherate (25 g, 0.046 mol if one ignores the contribution of the unknown amount of ether to the relative molar mass) was dissolved in 20 ml methanol. Tetra-butylammonium bromide (12.75 g, 0.039 mol), dissolved in 10 ml methanol, was added drop wise at room temperature over 15 min to the lithium solution. An off-white precipitate formed during this time. The septum-sealed suspension was then placed in a refrigerator at 0 °C for 30 min, after which it was transferred to a freezer at -25 °C where it was stored overnight. The precipitate that formed was removed by filtration from the brown liquid and washed with 10 ml cold (-25 °C) methanol and air dried before redissolving in distilled CH_2Cl_2 (30 ml). MgSO_4 was added to further dry the solution while stirring for 2 h at room temperature. The MgSO_4 was filtered off, washed with CH_2Cl_2 and the combined CH_2Cl_2 fractions were evaporated to liberate crude **1** as a white solid (21.7 g, 0.024 mol, 60%). Further purification by recrystallization was achieved as follows: to a solution of **1** (9 g, 0.01 mol) in 11 ml CH_2Cl_2 was added 55 ml ether drop wise, while stirring, over 20 min at room temperature. The septum-covered solution was cooled at 0 °C for an hour and then overnight at -25 °C. The precipitate was filtered off and washed with 30 ml of freshly distilled hexanes. The solid was air dried for 2 h and recrystallization was repeated for a second time. The product was then dried in vacuo for 3 days at 90 °C. 7.7 g of **1** was produced in this way. $\text{Mp} = 159\text{--}161$ °C. δ_{H} (300 MHz, CDCl_3)/ppm: 0.98 (t; 12H; $4 \times \text{CH}_3$); 1.36 (q, 8H; $4 \times \text{CH}_2$); 1.56 (q, 8H; $4 \times \text{CH}_2$); 3.03 (t, 8H; $4 \times \text{CH}_2$).

2.2.2. Synthesis of **4**

The reaction vessel was flame-dried and an argon atmosphere was maintained throughout. To a solution of acetyl ruthenocene (0.500 g; 1.8 mmol) in dry THF (1.2 ml) was added lithium diisopropylamide (1 cm³ of 1.8 mol dm⁻³ solution; 1.8 mmol) and the reaction mixture was stirred for 20 min while cooling on ice. Methyl ferrocenoate (0.44 g; 1.8 mmol) was added and the reaction mixture stirred for 16 h at room temperature before 35 cm³ of ether was added. The precipitate was collected by filtration, added to an ice-cold HCl solution (0.1 mol dm⁻³; 100 cm³) stirred for 5 min and the product extracted into ether. The ether layer was washed with H₂O (3 × 100 cm³), dried over MgSO₄, filtered and evaporated to dryness under reduced pressure. Chromatography over Kieselgel 60 (Merck, grain size 0.063–0.2 mm) of the residue with hexane:ether (1:4) (*R_f* = 0.53) as eluent gave **4** as red-brown crystals (294 mg; 34%), mp 178 °C; IR (cm⁻¹, neat) = 1606 (C=O). δ_{H} (300 MHz; CDCl₃): enol to the Fc side (47%), 5.9 (1H; s; COCHCO), 5.19 (2H; t; C₅H₄ Rc), 4.81 (2H + 2H Rc enol overlapping with Fc enol signal; t; C₅H₄), 4.60 (5H; s; C₅H₅ Rc), 4.51 (2H; t; C₅H₄ Fc), 4.20 (5H; s; C₅H₅ Fc); enol to Rc side (14%), 6.60 (1H; s; COCHCO), 5.14 (2H; t; C₅H₄ Rc), 4.81 (2H + 2H Rc enol overlapping with Fc enol signal; t; C₅H₄), 4.72 (2H; t; C₅H₄ Fc), 4.56 (5H; s; C₅H₅ Rc), 3.99 (5H; s; C₅H₅ Fc); keto (39%), 5.24 (2H; t; C₅H₄ Rc), 5.10 (2H; t; C₅H₄ Fc), 4.94 (2H + 2H Rc keto overlapping with Fc keto signal; t; C₅H₄ Rc), 4.61 (5H; s; C₅H₅ Rc) 4.23 (5H; s; C₅H₅ Fc) and 2.28 (2H; s; COCH₂CO). *Anal. Calc.* for C₂₃FeH₂₀O₂Ru: C, 56.77; H, 4.14. Found: C, 56.80; H, 4.16%.

2.3. Electrochemistry

Cyclic, linear sweep and Osteryoung square wave voltammetry were conducted using a computer-controlled BAS model 100 B/G potentiostat. Data, uncorrected for junction potentials, were collected with standard BAS 100 software and exported to Excel for manipulation and analyses. Temperature was controlled using a water bath at 20.0 ± 0.1 °C unless otherwise stated. Experiments were performed under argon on solutions of dried distilled CH₃CN, CH₂Cl₂ or THF in the presence of 0.1 mol dm⁻³ [N⁽ⁿ⁾Bu₄][PF₆], [N⁽ⁿ⁾Bu₄][B(C₆F₅)₄] or [N⁽ⁿ⁾Bu₄][B(C₆H₃(CF₃)₂)] as supporting electrolyte. A three-electrode cell containing a Pt-wire counter electrode was used. The BAS glassy carbon working electrode with surface area 3.14 or 7.07 mm² was pre-treated by polishing on a Buehler microcloth first with 1 μm and then ¼ μm diamond paste. The reference electrode was constructed from a silver wire inserted into a solution of 0.01 mol dm⁻³ AgNO₃ and 0.1 mol dm⁻³ [N⁽ⁿ⁾Bu₄][X] in CH₃CN in a luggin capillary with a vycor tip, [X] = [PF₆], [B(C₆F₅)₄] or [B(C₆H₃(CF₃)₂)]. For measurements in CH₂Cl₂ bulk solutions, this luggin capillary was inserted into a second luggin capillary with vycor tip filled with a 0.1 mol dm⁻³ [N⁽ⁿ⁾Bu₄][X] solution in CH₃CN to prevent Ag⁺ contact with CH₂Cl₂ and possible precipitation of AgCl. The working electrode was quickly contaminated and as a precaution it was washed (acetone, then methanol, then water) and polished between successive experimental groupings. It was never used for more than six successive cycles before it was recleaned. Successive experiments under the same experimental conditions showed that all formal reduction and oxidation potentials were reproducible to within 5 mV. Ferrocene and/or decamethylferrocene (Fc*) was added at the end of each experiment as internal standard to the bulk solution to enable data reporting vs. the Fc/Fc⁺ couple as recommended by IUPAC [9]. Under our experimental conditions, the Fc/Fc⁺ couple exhibited *E*^o = 0.087 V vs. Ag/Ag⁺, *i*_{pc}/*i*_{pa} = 0.98, Δ*E*_p = 74 mV in CH₃CN. In CH₂Cl₂, *E*_{Fc/Fc⁺}^o = 0.263 V vs. Ag/Ag⁺, *i*_{pc}/*i*_{pa} = 0.97, Δ*E*_p = 81 mV, while in THF it exhibited *i*_{pc}/*i*_{pa} = 0.97, Δ*E*_p = 86 mV and *E*^o = 0.176 V vs. Ag/Ag⁺. The Fc*/Fc*⁺ couple is at -0.610 V vs. Fc/Fc⁺ in CH₂Cl₂ as well as CH₃CN, while in THF the Fc*/Fc*⁺ couple is at -0.515 V vs. Fc/Fc⁺ [11].

3. Results and discussion

3.1. Complex **2**

Complex **2** has four redox-active ferrocenyl groups, and a Ru^{II}Ru^{III} core that can be irreversibly reduced to (Ru^{II})₂. In CH₂Cl₂/0.1 mol dm⁻³ [N⁽ⁿ⁾Bu₄][PF₆], utilising a glassy carbon working electrode, **2** at 1 mmol dm⁻³ concentrations showed a weak irreversible cathodic wave at -503 mV vs. Fc/Fc⁺ (not shown). The four ferrocenyl waves were located between 200 and 500 mV. This unresolved peak splitting of the anticipated four ferrocenyl waves is due to electrostatic effects of the differently charged oxidised ferrocenium and reduced ferrocenyl groups, and is indicative of intramolecular communication in **2**. However, resolution of the peaks into four separate redox steps was not observed in the PF₆-containing medium even though different formal reduction potentials for symmetrical complexes in which mixed-valent (i.e. differently charged) intermediates are generated are well known in systems that allow electron delocalisation, through through-space or through-bond conjugated paths [13,17,18]. This electrochemical behaviour mirrored very much the electrochemical profile in dichloroethane/[N⁽ⁿ⁾Bu₄][PF₆] of a similar compound in which only the ethanol axial ligands were replaced with 1-propanol, i.e. [Ru₂(μ-FcCOO)₄(CH₃CH₂CH₂OH)₂][PF₆], **5** [12]. The poorly resolved ferrocenyl electrochemical couples were also observed when the supporting electrolyte was changed to 0.10 mol dm⁻³ **1** (Fig. 2, top). However, upon lowering the concentration of **2** to 0.5 mmol dm⁻³, in the presence of 0.1 mol dm⁻³ **1**, all four ferrocene couples 1, 2, 3 and 4, could be resolved. OYSW voltammetry resolved the four ferrocenyl waves the best. Fig. 2 highlights the differences of the voltammograms of **2** under these concentration conditions while Table 1 summarises the electrochemical data that can be extracted from these voltammograms. This result highlights the key observation that higher concentrations (causing increasing non-ideal behaviour) may have a detrimental effect on peak resolution. A similar improvement in peak resolution was not observed in CH₂Cl₂/0.1 mol dm⁻³ [N⁽ⁿ⁾Bu₄][PF₆] when the concentration of **2** was halved.

A close inspection of Fig. 2 reveals that the Ru^{II}Ru^{III}/Ru^{II}Ru^{II} couple of **2** also behaved substantially different in CH₂Cl₂/[N⁽ⁿ⁾Bu₄][B(C₆F₅)₄] compared to what was previously described [12] for **2** in (1,2-C₂H₄Cl₂)/[N⁽ⁿ⁾Bu₄][PF₆]. On the cathodic cycle, the wave labelled "5" at -490 mV vs. Fc/Fc⁺ represents the irreversible Ru^{II}Ru^{III}/Ru^{II}Ru^{II} couple. However, this wave is followed by wave X. The LSV shows these two waves both represent the same amount of electrons. The insert CV labelled "CV with *i* × 2" shows that if the switching potential is not at 1000 mV, but at -200 mV, then on the second cathodic cycle, peak 5 disappeared. From this we conclude that **2** loosely coat the surface of the electrode after it was irreversibly reduced to completely modify the electrode surface. When the potential associated with wave X is reached, further molecules of **2** from the bulk of the solution are again reduced, but now at an electrode having markedly different characteristics than the original clean electrode.

That this adhesion of reduced **2** to the electrode surface is weak, is obvious from the main CV: if the switching potential is 1000 mV, by the time the next CV at faster scan rate is performed, the original electrode surface has already been regenerated, allowing once again observation of waves 1–4 in the expected positions.

3.2. Electrochemistry of **3**

The structure of **3** has been solved [15a]. To balance charges, one would expect **3** to have the formula [Cd₂H₂{Pc(C₆H₁₃)₈}₃]. However, no sign of the two protons to balance the charge of the three phthalocyanine rings could be found in the single crystal

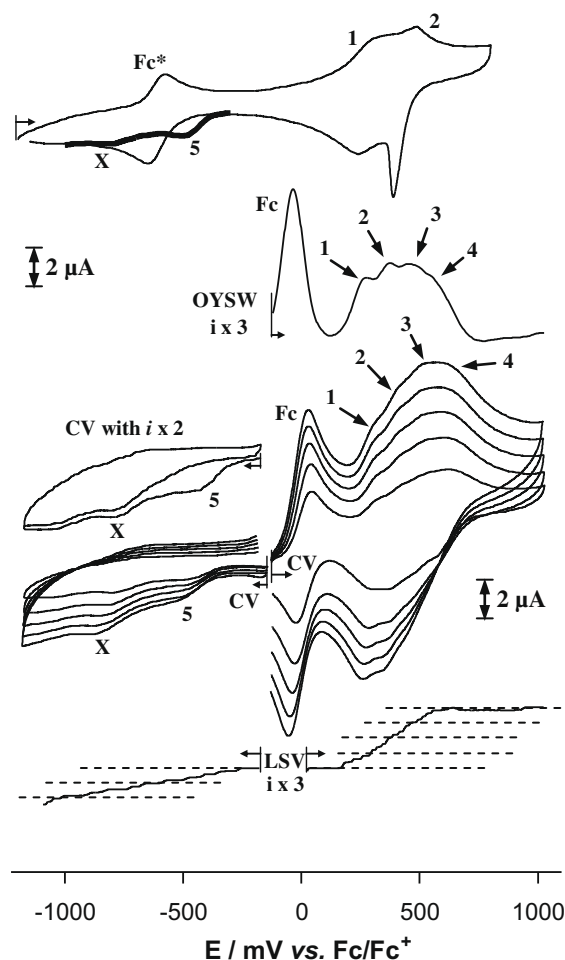


Fig. 2. Top: CV of **2** at 1 mmol dm^{-3} in $\text{CH}_2\text{Cl}_2/[\text{N}(\text{tBu})_4][\text{B}(\text{C}_6\text{F}_5)_4]$ with internal reference decamethylferrocene, Fc^* . The dark line highlights the Ru^{III} reduction at peak 5 in the absence of Fc^* . Bottom: LSV and CV's at 100 (smallest currents), 200, 300, 400 and 500 mV s^{-1} and a Osteryoung square wave voltammograms at 10 Hz of **2** at 0.5 mmol dm^{-3} .

structure determination. Complex **3** also shows so much radical content in the resting state [15], that it was impossible to obtain any NMR spectra. Until further light can be shed on the position of the two “missing” protons or the exact radical distribution of **3**, for the electrochemical discussion below, we choose to write this compound in the resting state as $\mathbf{3}^{2-} = [\text{Cd}_2\{\text{Pc}(\text{C}_6\text{H}_{13})_3\}]^{2-}$. In general, phthalocyanines with redox-silent metals in the cavity can exhibit two ring-based one-electron oxidations and four ring-based one-electron reductions [18]. Since cadmium is not redox-active, the investigated triple-decker phthalocyanine complex, **3**, can in principle show $2 \times 3 = 6$ one-electron transfer oxidation processes and $4 \times 3 = 12$ one-electron reductions. Regardless of solvent and supporting electrolyte, all six oxidation processes could be accounted for in waves A, B and C (Fig. 3). In CH_2Cl_2 , nine of the twelve reduction processes were identified in waves I through V. In THF, two further reduction processes could be identified, implying 17 of the possible 18 one-electron transfer processes that **3** can undergo, could be pinpointed. Although each of these processes should occur at a unique potential, some of them occurred at potentials so close to each other that they could not be resolved. The small CV peaks labelled X at -1.44 V and Y at 0.11 V vs. Fc/Fc^+ are not part of the main redox system associated with **3**. They are disassembled and different reassembled products of **3**, leading *inter alia* to metal free phthalocyanines and higher or-

der (tetra decker) species as described elsewhere [15]. Electrochemical data from these CV's is summarised in Table 2.

There were very noticeable differences in oxidation wave patterns upon moving from $\text{CH}_2\text{Cl}_2/[\text{N}(\text{tBu})_4][\text{B}(\text{C}_6\text{F}_5)_4]$ and $-\text{[B}(\text{C}_6\text{H}_3(\text{CF}_3)_2)_4]$ to $\text{CH}_2\text{Cl}_2/[\text{N}(\text{tBu})_4][\text{PF}_6]$ and $\text{THF}/[\text{N}(\text{tBu})_4][\text{B}(\text{C}_6\text{F}_5)_4]$. With the $\text{CH}_2\text{Cl}_2/[\text{N}(\text{tBu})_4][\text{B}(\text{C}_6\text{F}_5)_4]$ and $-\text{[N}(\text{tBu})_4][\text{B}(\text{C}_6\text{H}_3(\text{CF}_3)_2)_4]$ solvent/supporting electrolyte systems, the six possible oxidation one-electron transfer processes were detected in three separate oxidation waves labelled A, B and C (Fig. 3). From the LSV's each wave represents a total flow of two electrons. Utilising $[\text{N}(\text{tBu})_4][\text{PF}_6]$ as the supporting electrolyte, and also in the THF experiments, the six electron oxidation profile manifested in a different way. For the PF_6^- experiments, wave A still represented the first two oxidation processes, but waves B and C coalesced into closely overlapping peaks that in total represented the flow of four electrons. In THF, waves A and B each represented a flow of three electrons, and wave C was absent (Fig. 3). The first oxidation wave, wave A is in THF also shifted by 80 mV to more negative potentials than was found in CH_2Cl_2 solutions. Under oxidative conditions, oxidised products become more positive in character as demonstrated by $\mathbf{3}^{1+} \rightarrow \mathbf{3}^{4+}$, the four highest oxidised species of **3** (Scheme 1). Any species that can interact or associate with positively charged species will interact or associate with it. The oxidation profiles of **3** as demonstrated by the CV's of Fig. 3 are consistent with electrolyte anion PF_6^- interaction with **3**, probably via ion pair formation of the type $\mathbf{3}^{n+} \cdots (\text{PF}_6^-)$. THF presumably interacts via solvation to generate $\mathbf{3}^{n+} \cdots (\text{THF})_x$, $x \geq 1$. The contrasting oxidation patterns highlight how the larger volume of the $\text{B}(\text{C}_6\text{F}_5)_4^-$ and $\text{B}(\text{C}_6\text{H}_3(\text{CF}_3)_2)_4^-$ anions over that of PF_6^- as well as the electron withdrawing properties of the F-containing phenyl rings distributes the negative charge of $\text{B}(\text{C}_6\text{F}_5)_4^-$ anions over a large volume in comparison with PF_6^- . The effect of this lower charge density is to minimise ion pair formation and enhance observation of electron transfer processes associated with naked cations.

Cyclic voltammetry could not resolve any of the two processes associated with waves A, B or C in any of the four solvent/electrolyte mediums used, but an Osteryoung square wave analyses in $\text{CH}_2\text{Cl}_2/[\text{N}(\text{tBu})_4][\text{B}(\text{C}_6\text{H}_3(\text{CF}_3)_2)_4]$ (not shown) or $\text{CH}_2\text{Cl}_2/[\text{N}(\text{tBu})_4][\text{B}(\text{C}_6\text{F}_5)_4]$ (Fig. 3) clearly demonstrated the two components of wave C. Wave A did not resolve into two separate peaks with the square wave technique, but a shoulder next to the main peak in the presence of **1** is observable. In CH_2Cl_2 , wave B did not resolve in any form of resolution associated with the two steps with any of the techniques at our disposal.

The small degree of peak-overlap in wave B is emphasised with the CV $\Delta E_{\text{B}(\text{C}_6\text{F}_5)_4} \leq 96 \text{ mV}$. For wave A, the CV $\Delta E_{\text{A}(\text{B}(\text{C}_6\text{F}_5)_4)} = 128 \text{ mV}$. This slightly larger $\Delta E_{\text{A}(\text{B}(\text{C}_6\text{F}_5)_4)}$ value explains why a shoulder on the main peak of A could be observed in the square wave and CV voltammograms. The portion of the CV's associated with wave C in $\text{CH}_2\text{Cl}_2/[\text{N}(\text{tBu})_4][\text{B}(\text{C}_6\text{F}_5)_4]$ and $-\text{[B}(\text{C}_6\text{H}_3(\text{CF}_3)_2)_4]$ gave $\Delta E_{\text{C}} \geq 190 \text{ mV}$ and is completely consistent with two near overlapping peaks that could be resolved by OYSW voltammetry. Which two of the three phthalocyanine rings **3** is first oxidised (or reduced) could not be unambiguously identified. The above-mentioned relatively small ΔE values – each applies to two one-electron transfer processes, not only one – lead us to conclude that all six one-electron oxidations should be to a large extent electrochemically reversible and fast on the CV time scale.

For the reduction processes of **3** the observed electrochemistry in $\text{CH}_2\text{Cl}_2/[\text{N}(\text{tBu})_4][\text{B}(\text{C}_6\text{F}_5)_4]$, $-\text{[B}(\text{C}_6\text{H}_3(\text{CF}_3)_2)_4]$ and $-\text{[PF}_6]$ paralleled each other very closely implying ion pair formation between the anions of these electrolyte anions and negatively charged reduced forms of **3** is negligible. Only cations would influence reduction process of anionic species by ion pairing of the type (anionic species) $^- \cdots ^+(\text{cation})$. LSV peaks I, II and III showed each of these waves are associated with a one-electron transfer process. That

Table 1

Voltammetry data for **2** and **4** at scan rate = 100 mV s⁻¹ of ca. 1.0 mol dm⁻³ solutions of compounds at 20 °C. Potentials are vs. Fc/Fc⁺.

Wave	E_{pa} (V)	ΔE_p (mV)	E° (V)	i_{pa} (μ A)	i_{pc}/i_{pa}^a	Wave	E_{pa} (V)	ΔE_p (mV)	E° (V)	i_{pa} (μ A)	i_{pc}/i_{pa}^a
Ferrocene, Fc						Decamethylferrocene, Fc*					
In CH ₃ CN	0.037	74	0	2.32	0.98	In CH ₃ CN	-0.575	70	-0.61	2.12	0.99
In CH ₂ Cl ₂	0.041	81	0	2.08	0.97	In CH ₂ Cl ₂	-0.576	68	-0.61	2.04	0.99
In THF	0.043	86	0	2.90	0.97	In THF	-0.468	82	-0.515	2.94	0.96
2 (1.0 mM) in CH₂Cl₂/[N^{(t}Bu)₄][B(C₆F₅)₄]						2 (0.5 mM) in CH₂Cl₂/[N^{(t}Bu)₄][B(C₆F₅)₄]					
1	0.292	60	0.257	0.7 ^b	0.9 ^b	1	0.324	60	0.294	0.7 ^b	0.9 ^b
2	0.462	94	0.415	0.7 ^b	0.9 ^b	2	0.434	74	0.397	0.7 ^b	0.9 ^b
3	— ^c	— ^c	— ^c	— ^c	— ^c	3	0.526	76	0.488	0.7 ^b	0.9 ^b
4	— ^c	— ^c	— ^c	— ^c	— ^c	4	0.626	66	0.593	0.7 ^b	0.9 ^b
5	-0.503 ^d	—	0.593	0.4 ^d	—	5	-0.495 ^d	—	—	0.4 ^d	—
X	— ^e	—	—	—	—	X	-0.787	—	—	0.3	—
4 in CH₃CN/N^{(t}Bu)₄PF₆						4 in CH₂Cl₂/[N^{(t}Bu)₄][B(C₆F₅)₄]					
Enol Fc, 1	0.176 ^f	ca. 74 ^f	0.213	11.2 ^b	— ^c	Enol Fc, 1	0.154	ca. 111	0.213	10.6 ^f	— ^c
Keto Fc, 2	0.207	ca. 74 ^f	0.244	10.6 ^b	— ^c	Keto Fc, 2	0.203	ca. 111	0.258	9.4 ^f	— ^c
Enol Rc, 3	0.484	— ^c	— ^c	11.4 ^b	— ^c	Enol Rc, 3	0.802	ca. 131	0.737	— ^c	— ^c
Keto Rc, 4	0.636	— ^c	— ^c	11.2 ^b	— ^c	Keto Rc, 4	0.883	ca. 106	0.83	— ^c	— ^c
Dimer, 5	— ^c	— ^c	— ^c	— ^c	— ^c	Dimer, 5	0.515 ^g	— ^c	— ^c	— ^c	— ^c

^a Current ratios were always taken to be (reverse scan current)/(forward scan current).

^b Estimates only.

^c Not observed, or poor peak resolution disallowed accurate peak current measurement.

^d E_{pc} or i_{pc} (no E_{pa} were detected).

^e It is unclear if the shoulder at -0.83 V actually is peak X as observed when [2] = 0.5 mmol dm⁻³.

^f Due to poor peak resolution, E_{pa} could not be measured, $E_{pc,1}$ = 0.176 V. Upon assuming ΔE_p = 74 mV, as was found for free ferrocene under our conditions, E_{pa} could be estimated, and formal reduction potential estimates are $E_1^{\circ} \approx 0.213$ and $E_2^{\circ} \approx 0.244$ V vs. Fc/Fc⁺.

^g An E_{pc} value. In CH₂Cl₂, a weak reduction process was observed which is attributed to a dimerized Ru^{III} species in analogy with what was found for free ruthenocene. At 0 °C this peak was absent and wave 3 became dominant in the cathodic cycle.

Table 2

Voltammetry data of ca. 0.5 mM solutions of **3** at -40 °C in CH₂Cl₂ or THF containing 0.1 M [N^{(t}Bu)₄][B(C₆H₅)₄], [NBu₄][B(C₆H₃(CF₃)₂)₄] or [N^{(t}Bu)₄][PF₆].

Wave	LSV ^a n^b	CV ^c E_{pc} (V)	CV ΔE_p (mV)	CV ^c E° (V)	OYSW ^{c,d} E (V)	Wave	LSV n^b	CV ^c E_{pc} (V)	CV ΔE_p (mV)	CV ^c E° (V)	OYSW ^{c,d} E (V)
3, in CH₂Cl₂/[N^{(t}Bu)₄][B(C₆F₅)₄]						3, in THF/[N^{(t}Bu)₄][B(C₆F₅)₄]					
VI	— ^e	— ^e	— ^e	— ^e	— ^e	VI	2	-2.89	140	-2.82	-2.83
V	2 or 3	-2.21	90	-2.16	-2.13(-2.18) ^f	V ₃	1	-2.51	110	-2.45	-2.47
	— ^e	— ^e	— ^e	— ^e	— ^e	V ₂	1	-2.36	150	-2.28	-2.31
	— ^e	— ^e	— ^e	— ^e	— ^e	V ₁	1	-2.23	80	-2.19	-2.23
IV _{1,2}	3	-1.86	170	-1.78	-1.79(-1.87) ^f	IV ₃	1	-1.96	140	-1.89	-1.93
III	1	-1.10	62	-1.07	-1.09	IV _{1,2}	2	-1.82	130	-1.75	-1.77
II	1	-0.72	86	-0.68	-0.7	III	1	-1.12	139	-1.05	-1.07
I	1	-0.53	76	-0.49	-0.5	II	1	-0.85	204	-0.75	-0.71
						I	1	-0.65	228	-0.54	-0.53
A	2	-0.11 ^g	128	-0.17	-0.18(-0.11) ^f	A	3	-0.20 ^g	100	-0.25	-0.22
B	2	0.47 ^g	92	0.42	0.44	B ₁	3 ^h	0.35 ^g	196	0.25	0.3
C	2	0.91 ^g	220	0.80	0.78(0.91) ^f	B ₂	3 ^h	0.49 ^g	160	0.41	0.43
3, in CH₂Cl₂/[NBu₄][B(C₆H₃(CF₃)₂)₄]						3, in CH₂Cl₂/[N^{(t}Bu)₄][PF₆]					
V	2 or 3	-2.18	90	-2.13	-2.16	V	2 or 3	-2.21	90	-2.16	-2.17
IV	3	-1.77	150	-1.7	-1.69	IV	3	-1.86	160	-1.78	-1.81
III	1	-1.08	92	-1.03	-1.05	III	1	-1.11	62	-1.08	-1.07
II	1	-0.72	92	-0.67	-0.68	II	1	-0.72	88	-0.68	-0.65
I	1	-0.52	76	-0.48	-0.5	I	1	-0.53	80	-0.49	-0.48
A	2	-0.08 ^g	120	-0.14	-0.15	A	2	-0.10 ^g	118	-0.16	-0.15
B	2	0.52 ^g	82	0.48	0.48	B	4	0.47 ^g	96	0.42	0.45
C	2	0.92 ^g	190	0.82	0.77(0.91) ^f	C	—	0.82 ^g	120	0.76	0.78

^a LSV recorded at a scan rate of 2 mV s⁻¹.

^b Amount of electrons that flowed per molecule of **3** for each wave as determined by LSV.

^c Scan rate = 100 mV s⁻¹; potentials vs. Fc/Fc⁺ = 0 mV in CH₂Cl₂ or at -0.095 in THF; under these conditions, the Fc⁺/Fc²⁺ couple is at -610 mV in both solvents used, see Table 1.

^d Osteryoung square wave recorded at 10 Hz.

^e Peak not observed in this solvent.

^f First-mentioned potentials are those of the of the first identifiable peak, the potential in brackets are for the second identifiable peak or shoulder associated with the main peak.

^g E_{pa} not E_{pc} .

^h The total amount of electrons that flows per molecule at wave B_{THF}.

the region between waves A and I really represents the resting state of **3** under the oxygen free conditions in the glove box, is clearly proved by the CH₂Cl₂ LSV of Fig. 3. It is only in the potential range between waves I and A that the LSV experiment drew zero current.

ΔE values for I–III from the CV scans at 100 mV s⁻¹ were all below 92 mV indicating near electrochemically reversible processes. Another observation that supported this conclusion was the observation that peak potentials was independent of scan rate. This

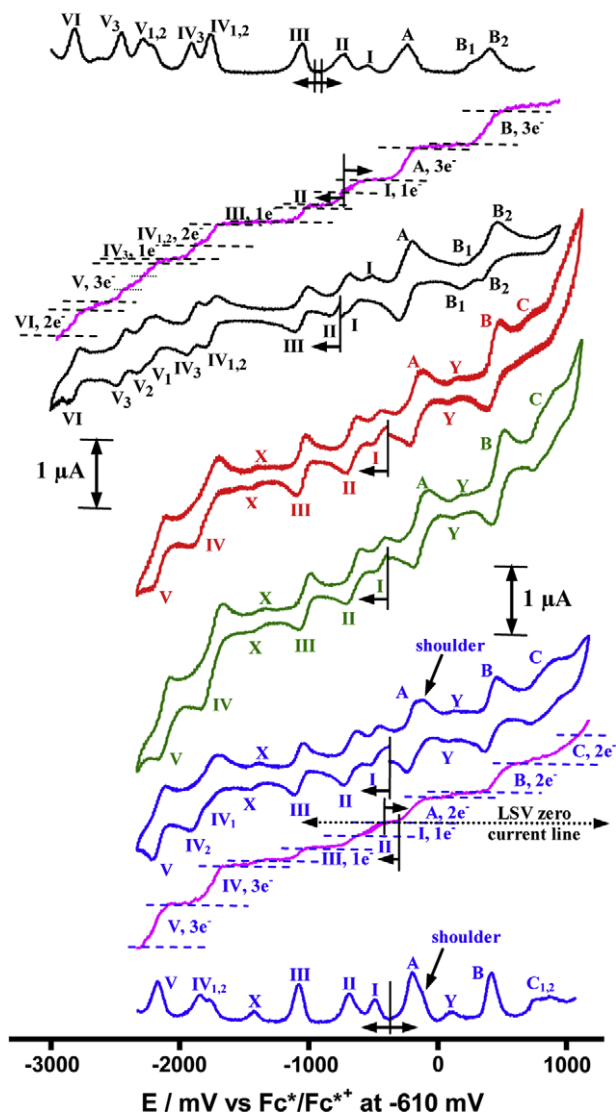
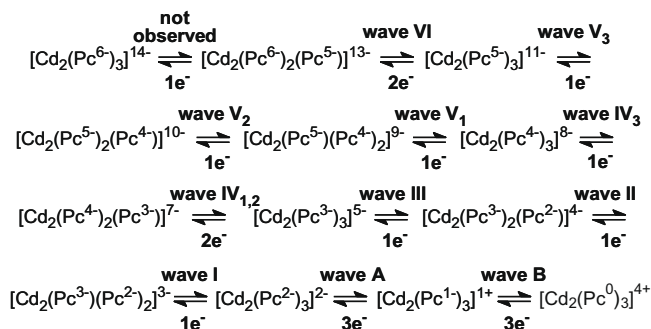


Fig. 3. CVs at 100 mV s⁻¹ and -40 °C highlighting the differences in oxidation waves A–C due to solvent or electrolyte changes. Reduction processes are labelled I through VI, numbering start from the resting potential to synchronize wave number with sequential redox processes. **Blue:** OYSW and CV of a 0.5 mM solution of **3** in CH₂Cl₂/[N(ⁿBu)₄][B(C₆F₅)₄]. **Green:** CV in CH₂Cl₂/[N(ⁿBu)₄][B(C₆H₃(CF₃)₂)₄]. **Red:** CV in CH₂Cl₂/[N(ⁿBu)₄][PF₆]. **Black:** CV and OYSW in THF/[N(ⁿBu)₄][B(C₆F₅)₄]. **Purple:** LSVs at 2 mV s⁻¹ in CH₂Cl₂ or THF. The experimentally measured LSV currents were multiplied by 2 for better display purposes; the dotted lines accentuate the electron count associated with each wave and pinpoint the resting position of **3**. The reference potential was taken as -610 mV for the Fc⁺/Fc⁰ couple. This implies data is also referenced vs. Fc⁺/Fc⁰ = 0 V in CH₂Cl₂ but not in THF. In THF, the Fc⁺/Fc⁰ couple is at -80 mV under these conditions, Table 1. The peaks labelled Y and X are not part of the electrochemical fingerprint of **3**, see text. (For interpretation of the references in colour in this figure legend, the reader is referred to the web version of this article.)

cluster of the first three reduction processes represents the first reduction wave on each phthalocyanine ring of **3** and is better resolved than any other cluster of three one-electron transfer process associated with **3**. The other peaks in the CV of **3** all represented to a large degree electron transfer processes consisting of coalesced peaks. The good resolution between peaks I, II and III is indicative of an enhanced field effect through through-space communication [17] between the differently charged intermediate reduced species **3**²⁻, **3**³⁻, **3**⁴⁻ and **3**⁵⁻ (Scheme 1). Here, the different charges are located on the neighbouring phthalocyanine rings which are only 2.965 Å apart [15a].



Scheme 1. Seventeen of the possible one-electron transfer processes for **3** could be identified in THF according to the reaction sequence above.

In THF, waves I, II and III, are also representative of the first three one-electron transfer processes of **3** to generate **3**³⁻, **3**⁴⁻ and **3**⁵⁻, respectively. The set of formal reduction potentials I–III were within 70 mV of those obtained in CH₂Cl₂ (Table 2). Although THF interacted strongly with positively charged oxidised species of **3**, THF interaction with the large negatively charged reduced forms of **3** that is generated in waves I through VI was negligible. The reduced forms of **3** vary between **3**³⁻ and the fully reduced species **3**¹⁴⁻ (Scheme 1).

In contrast to waves I–III, by virtue of the LSV traces, both waves IV and V in all CH₂Cl₂ experiments represent a cluster of three one-electron transfer processes. The three one-electron transfer processes associated with wave IV are better resolved than in wave V, because ΔE_{IV} is 70–80 mV larger than ΔE_V = 90 mV (Table 2). This larger peak separation also allowed the OYSW technique to resolve wave IV in the presence of **1** into two of its three components (Fig. 3). No evidence for the fourth array of reduction processes was found in CH₂Cl₂ as solvent, but evidence for this step was found in THF.

When wave IV_{THF} was encountered, it was found to be well enough resolved to separate two of the three expected one-electron transfer processes. From the LSV scans, the combined amount of electrons that was transferred during the overall processes associated with wave IV were still three. OYSW voltammetry could still not resolve wave IV into three separate peaks. However, in THF, wave V clearly split into all three its components during generation of **3**⁹⁻, **3**¹⁰⁻ and **3**¹¹⁻, respectively. The OYSW trace shown in Fig. 3 highlights the higher degree of resolution in THF best. Part of the reason why wave V resolved into its three separate components must centre around a very low degree of interaction between **3**ⁿ⁻ and THF under strong reducing conditions. However, this is not the only reason. A second contributing factor as to why this happened lies in the slower rate of electron transfer between **3**ⁿ⁻, and the working electrode in THF. From Table 2 it is clear that ΔE values are almost always smaller in CH₂Cl₂ than in THF. This means that electron transfer between **3** and the working electrode is much faster in CH₂Cl₂ than in THF (fast electrochemical reversible processes are theoretically characterised by ΔE = 59 mV [1]). It implies that measured peak potentials in THF are not necessarily thermodynamically ideal. Rather, they are shifted in such a way that peak potentials represent the potentials where the fastest rates of electron transfer occur. This induced quasi electrochemical reversibility in THF and contributed to the chance observation of three separate one-electron transfer peaks for wave V and two of three possible peaks for wave IV.

The final additional feature introduced by the use of THF as solvent was observation of the fourth and final possible reduction wave set associated with **3** in wave VI. Wave VI could not be

observed in CH_2Cl_2 as it occurred outside the potential window of this solvent. The LSV scans showed wave VI to comprise of at least two one-electron transfer processes, thus generating $\mathbf{3}^{12-}$ and $\mathbf{3}^{13-}$. The onset of solvent decomposition at this low potential made it uncertain if the final reduction to $\mathbf{3}^{14-}$ could be detected. OYSW analyses could not resolve the two observed processes into separate steps. The strength of the cadmium bonds to the phthalocyanine macrocycles are put into perspective when one observes that $\mathbf{3}^{13-}$ did not dissociate to monomeric or dimeric species due to electrostatic repulsive forces on the CV time scale.

In order to write a reaction sequence for the described electrochemistry in THF, it is useful to recognising that the charge of Cd is 2+ and that of the hydrogen-free phthalocyaninato (Pc) rings is 2-. The resting state of $\mathbf{3}$ can then be written as $[\text{Cd}_2(\text{Pc}^{-2})_3]^{2-}$. In this notation, the charge in the bracket represents the charge on an individual Pc ring while the outer charge represents the total charge on the molecule. By adopting this writing style, Scheme 1 can be written to describe the 17 observed and 1 unobserved electrochemical processes of $\mathbf{3}$ in THF as solvent.

3.3. Electrochemistry of $\mathbf{4}$

The β -diketone $\mathbf{4}$ exists as an equilibrium of enol and keto isomers as described elsewhere [14]. Freshly prepared samples have a high keto content, but in the solid state, samples of $\mathbf{4}$ convert within a few weeks exclusively to the enol form. Upon dissolving an aged, enol-enriched solid sample, it slowly converts to the equilibrium keto-enol position over several hours. The kinetics of this conversion have been studied, [14]. In CH_3CN , the ferrocenyl centre of $\mathbf{4}$ showed reversible electrochemistry with the formal reduction potentials of the two poorly resolved waves estimated at $E^\circ = 0.213$ for the enol isomer (wave 1, Fig. 4, left, top, from an aged sample of $\mathbf{4}$) and 0.244 V for the keto isomer (wave 2, from a sample of $\mathbf{4}$ at equilibrium). E° was calculated by assuming $\Delta E_p = 74$ mV for both waves, the same as that for free ferrocene, at a scan rate of 100 mV s^{-1} (Table 1, Fig. 4). In contrast, irreversible electrochemistry was found for the ruthenocenyl centre of $\mathbf{4}$ in CH_3CN in the presence of $0.1 \text{ mol dm}^{-3} [\text{N}(\text{tBu})_4][\text{PF}_6]$ supporting electrolyte. Only anodic peak potentials for the enol (wave 3)

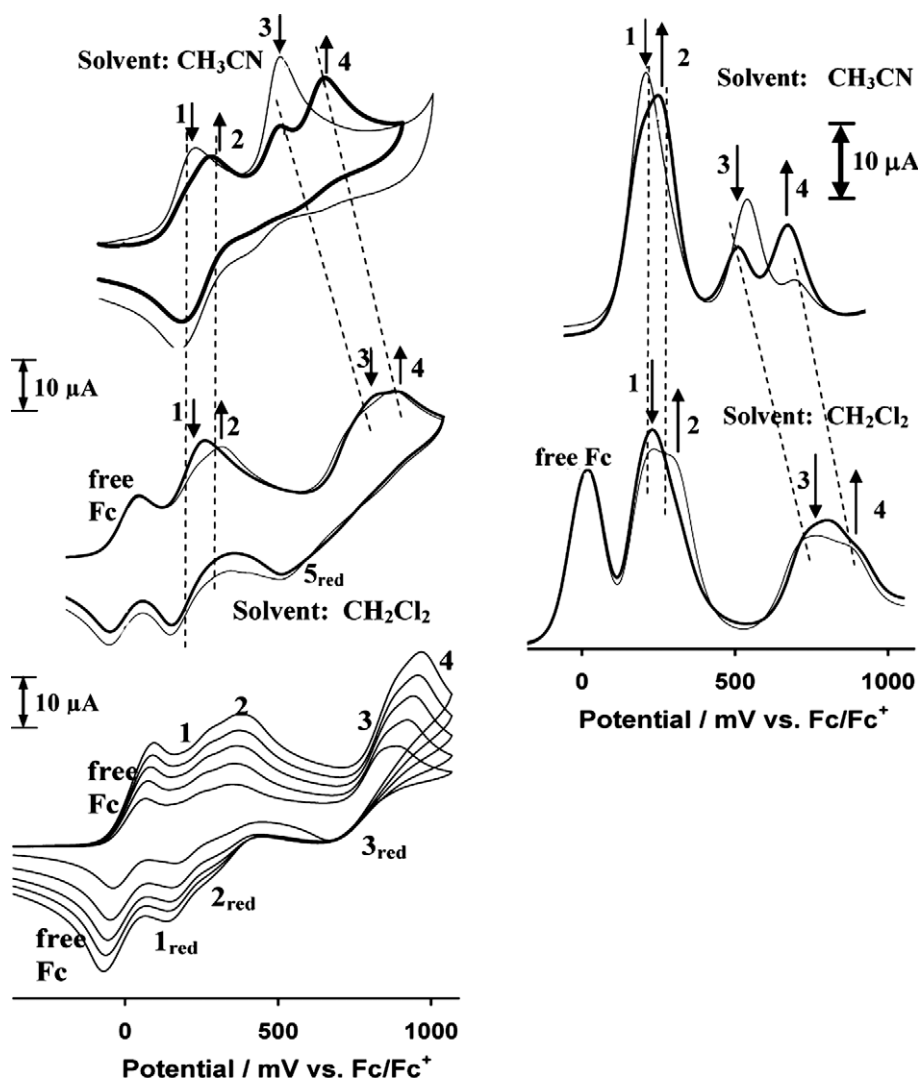


Fig. 4. Left. Top: Enol-enriched (thin line) and equilibrium enol/keto content CV's at 100 mV/s of **4** in CH_3CN at 20 °C. Middle: Enol-enriched (thick line) and equilibrium enol/keto content CV's of **4** in CH_2Cl_2 at 20 °C. The reduction half wave 5_{red} at 515 mV is associated with isomers of a hydride-containing dimer similar to that found for ruthenocene, i.e. $[(\text{H})(\text{C}_5\text{H}_5)\text{Ru}^{\text{III}}(\text{C}_5\text{H}_4)_2]$ [21]. Bottom: CV's at 0 °C in CH_2Cl_2 of an equilibrium solution of **4** at scan rates of 100 (smallest currents), 200, 300, 400 and 500 mV. The reduction half wave 3_{red} at ca. 662 mV is associated with a simple $(\text{C}_5\text{H}_5)\text{Ru}^{\text{II}}(\text{C}_5\text{H}_4\text{R})/(\text{C}_5\text{H}_5)\text{Ru}^{\text{III}}(\text{C}_5\text{H}_4\text{R})$ couple overlapping the two-electron reduction wave of isomers of $[(\text{C}_5\text{H}_4\text{R})(\text{C}_5\text{H}_5)\text{Ru}^{\text{III}}-\text{Ru}^{\text{III}}(\text{C}_5\text{H}_5)(\text{C}_5\text{H}_4\text{R})]^{2+}$. Right: OYSW voltammograms of **4** at 10 Hz and 20 °C of **4** and at equilibrium in CH_3CN (top; thin line enriched in the enol form; thick line for an equilibrium keto-enol solution of **4**) or CH_2Cl_2 (bottom, thick line enriched in the enol form, thin line of keto/enol equilibrium solutions).

and keto forms (wave 4) of **4** were observed at 0.484 and 0.636 V, respectively. It is generally accepted that Ru^{IV} species arise in CV experiments involving ruthenocene derivatives in CH₃CN/[N(ⁿBu)₄][PF₆] [8g,14,19,20]. Here, in analogy to free ruthenocene [14,21] and also free osmocene [22], [(C₅H₄R)(C₅H₅)Ru^{IV}(CH₃CN)]²⁺ is probably formed, R = {CO–CH₂–CO–Fc ⇌ CO–CH=C(OH)–Fc}.

However, Mann and co-workers [8g], and more recently Geiger and co-workers [8b,21], reported reversible oxidation of free ruthenocene in CH₂Cl₂/[N(ⁿBu)₄][B((C₆H₃(CF₃)₂)₄)] and CH₂Cl₂/[N(ⁿBu)₄][B(C₆F₅)₄] to two Ru^{III} species, one the simple monomeric ruthenocenium cation [(C₅H₅)₂Ru^{III}]⁺, the other dimeric [(C₅H₅)₂Ru^{III}–Ru^{III}(C₅H₅)₂]²⁺ which exists at low (–40 to 0 °C) temperature. At higher temperature this dimer can isomerise reversibly to the hydride-containing dimer [(H)(C₅H₅)Ru^{III}(C₅H₄)₂]²⁺ which also has a Ru–C σ-bond [21]. The ruthenocene-containing β-diketone **4** behaved similarly.

Upon comparing electrochemical results of **4** from a CH₃CN medium with those obtained in CH₂Cl₂ (Table 1, Fig 4), a key observation is that, although formal reduction potentials vs. Fc/Fc⁺ for ferrocenyl-based waves 1 and 2 are for all practical purposes the same in both solvents, potentials for waves 3 and 4 of the ruthenocenyl group of **4** shifted to much more positive values; from 0.484 and 0.636 V to 0.802 and 0.883 V, respectively. In CH₃CN, Δ*E*_{pa,Rc} = *E*_{pa,wave 4} – *E*_{pa,wave 3} = 152 mV for the ruthenocenyl fragment, while in CH₂Cl₂ Δ*E*_{pa,Rc} is only 81 mV. This value is almost the same as that of the ferrocenyl group in CH₂Cl₂ where Δ*E*_{pa,Fc} = *E*_{pa,wave 2} – *E*_{pa,wave 1} = 50 mV. Hence, different ruthenocene oxidation products form in CH₂Cl₂ and CH₃CN. The closeness of the Δ*E*_{pa,Fc} and Δ*E*_{pa,Rc} values in CH₂Cl₂ is consistent with keto and enol forms of **4** also forming the simple but labile, monomeric ruthenocenium cations [(C₅H₅)Ru^{III}(C₅H₄R)]⁺ at the anodic half-waves 3 and 4, just as the ferrocenyl group is involved in the simple redox couple [(C₅H₅)Fe^{III}(C₅H₄R)]⁺/[(C₅H₅)Fe^{II}(C₅H₄R)] at waves 1 and 2. In CH₃CN, [(C₅H₄R)(C₅H₅)Ru^{IV}.CH₃CN]²⁺ forms. For the ruthenocenyl fragment, Eqs. (1)–(4) are only valid in CH₂Cl₂/[N(ⁿBu)₄][B(C₆F₅)₄].

The *i*_{pc}/*i*_{pa} current ratio for waves 3 and 4 in CH₂Cl₂ deviate substantially from unity. Results therefore indicate that the oxidised enol and keto [(C₅H₅)Ru^{III}(C₅H₄R)]⁺ fragments are prone to further chemical processes. At 20 °C, the position of the most prominent [(C₅H₅)Ru^{III}(C₅H₄R)]⁺ fragment reduction wave at *E*_{pa} = ca. 0.515 V vs. Fc/Fc⁺ in CH₂Cl₂ (Fig. 4, left middle), is consistent with a two-electron Ru^{III} dimer reduction in analogy to free ruthenocene [8b,21], because it is found at a potential ca. 290 mV lower than *E*_{pa} = 802 mV for peak 3. This peak potential difference is too large to be associated with a simple [(C₅H₅)Ru^{III}(C₅H₄R)]⁺/[(C₅H₅)Ru^{II}(C₅H₄R)] couple. However, weak peak shoulders 3_{red} and 4_{red} are observed at ca. *E*_{cathodic} = ca. 671 and 777 mV. The estimated Δ*E*_p = *E*_{pa,peak i} – *E*_{pc,shoulder i} values of ca. 131 and 106 mV for peak/shoulder pairs 3 and 4 point to quasi reversible simple [(C₅H₅)Ru^{III}(C₅H₄R)]⁺/[(C₅H₅)Ru^{II}(C₅H₄R)] couples, but a plot of the square root of scan rate, (ν)^{0.5}, vs. peak anodic currents was found to be linear for waves 3 and 4 in CH₂Cl₂ (Fig. 5). Thus, ruthenocenyl oxidation of **4** in CH₂Cl₂ obeys Eq. (4), indicating electrochemical reversibility even though the [(C₅H₅)Ru^{III}(C₅H₄R)]⁺ cation is chemically converted to a dimeric species in a chemical process directly after ruthenocene oxidation. This result highlights the difference between electrochemical reversibility and chemical reversibility. Chemical irreversibility implies *i*_{pc}/*i*_{pa} current ratios deviate from unity even though the electron transfer process may still be electrochemically reversible. In contrast, in CH₃CN, *i*_{pa}–(ν)^{0.5} plots for waves 3 and 4 deviated from linearity, thereby confirming ruthenocenyl oxidation in CH₃CN is not an electrochemically reversible process. A repeat CV experiment in CH₂Cl₂ performed not at 20 °C but at 0 °C confirmed a strong reduction peak associated with wave 3 at 662 mV vs. Fc/Fc⁺ but no dimer reduc-

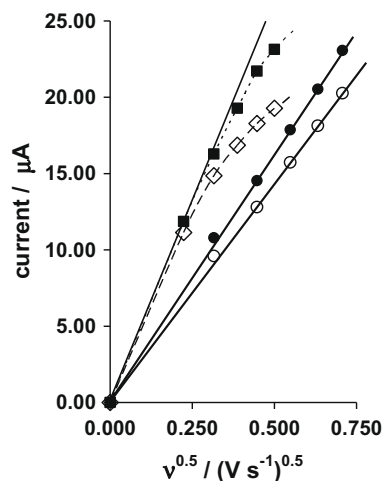
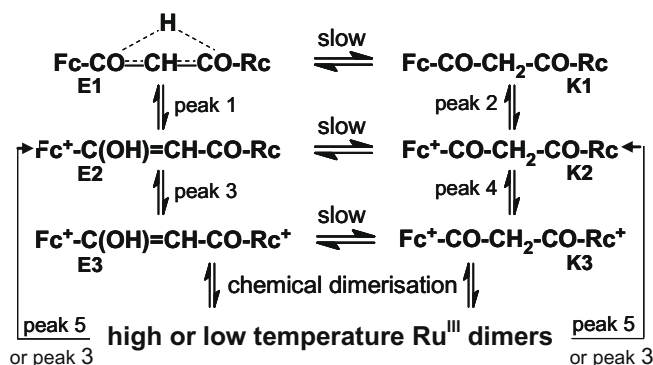


Fig. 5. The relationship between *i*_{pa} and square root of scan rate, ν^{0.5}, Eq. (4), deviates from linearity in waves 3 (dotted line, ■) and 4 (broken line, ◇) of **4** in CH₃CN, demonstrating electrochemical irreversibility. In contrast, in CH₂Cl₂, this relationship is linear. Graph shows wave 3 (●) and the superimposed current of waves 3 and 4 (○; current at *E*_{pa,wave 4}). Poor wave resolution, prevented determination of accurate *i*_{pa} values for wave 4 alone.

tion peak at ca. 515 mV vs. Fc/Fc⁺ (Fig. 4, bottom left). In analogy to free ruthenocene [8b,21], this reduction wave is considered to represent the two-electron reduction of isomers of the low temperature Ru^{III} dimer [(C₅H₄R)(C₅H₅)Ru^{III}–Ru^{III}(C₅H₅)(C₅H₄R)]²⁺ overlapping with small amounts of simple monomeric [(C₅H₅)Ru^{III}(C₅H₄R)]⁺ reduction. That wave 3_{red} is associated with the reduction of monomeric and dimeric forms of **4** in equilibrium are also borne out by the shape of this peak and its scan rate dependence. At low sweep rates peak 3_{red} is rather sharp because the rate of the equilibration process can keep up with the rate of the electrochemical experiment. As the sweep rate increases, the electrochemical process “outruns” the dimer-monomer equilibrium. This renders peak 3_{red} broad, drawn out and weak with the results that the peak currents associated with back-reduction do not increase in the same manner as currents in the forward peak. The OYSW voltammograms of **4** are shown in Fig. 4, right, and better resolution of especially the ferrocenyl waves were observed.

Utilising the above CH₂Cl₂ results, Scheme 2 can be written for **4** to involve electrochemically reversible one-electron oxidation processes during the generation of enol and keto isomers E1–E3 and K1–K3 at waves 1, 2, 3 and 4, respectively. At 20 °C, a two-electron reduction of isomers of a Ru^{III} dimer back to the ruthenocenyl group is associated with wave 5_{red}. With present knowledge, the dimer is most likely isomers of the hydride-containing dimer



Scheme 2. Electron transfer processes associated with **4**.

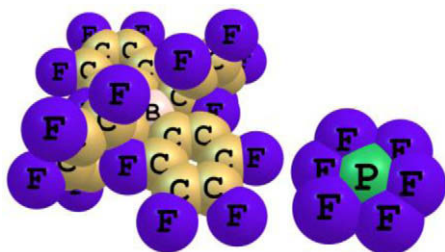


Fig. 6. Space filling diagram of $B(C_6F_5)_4^-$ and PF_6^- anions. The longest distance between diagonal F-atoms on $B(C_6F_5)_4^-$ and PF_6^- anions approach 10 and 3.3 Å, respectively.

$[(H)(C_5H_5)Ru^{III}(C_5H_4)]_2$ which also has a Ru–C σ -bond, similar in structure to what was found for free ruthenocene [21] and analogous free osmocene [22]. At 0 °C, a two-electron reduction of isomers of the Ru^{III} dimer $[(C_5H_4R)(C_5H_5)Ru^{III}-(C_5H_5)(C_5H_4R)]^{2+}$ back to the ruthenocenyl species is associated with wave 3_{red} .

The species E1 is considered to be reduced at lower potentials than K1, because carbonyl (C=O) substituted metallocenes are oxidised at larger (more positive) potentials than alcohol (OH) substituted metallocenes [17e].

All of the above described results were made possible by the uses of the $CH_2Cl_2/[N^{(t)Bu}_4][B(C_6F_5)_4]$ solvent electrolyte system to minimise ion pairing interactions between electrolyte anions and positively charged oxidised substrates, and by careful choice of the solvent. Fig. 6 shows a space filling diagram of the $B(C_6F_5)_4^-$ and PF_6^- anions generated by the program Chemcraft on the same scale.

Upon visualising the size and structure of the $[B(C_6F_5)_4]^-$ anion, it is easy to comprehend how the negative charge on $[B(C_6F_5)_4]^-$ can be distributed over a much larger volume than in $[PF_6]^-$ because of the electron withdrawing effects of each of the C_6F_5 groups, thereby leading to a much smaller charge density on the anion.

4. Conclusions

In this paper we have clearly shown how the use of $CH_2Cl_2/[N^{(t)Bu}_4][B(C_6F_5)_4]$ as solvent/supporting electrolyte results in better resolution and a clearer electrochemical picture of multiple redox processes associated with positively charged analytes. Under strong reducing conditions, the larger negative potential window of THF can append results from CH_2Cl_2 , especially if the analyte becomes positively charged upon reduction. In $CH_2Cl_2/[N^{(t)Bu}_4][B(C_6F_5)_4]$ the complex $[Ru_2(\mu-FcCOO)_4(\cdot CH_3CH_2OH)_2][PF_6]$, **2**, exhibited all four Fc/Fc⁺ couples in well-resolved form, while in the presence of PF_6^- , they coalesced into two groups of electron transfer processes. For the biscadmium trisphthalocyaninato complex **3**, all six possible oxidation processes could be identified. Solvent coordination by THF and ion pair formation between positively charged oxidised species of **3** and PF_6^- distorted the oxidation wave pattern. The most meaningful oxidation studies with positively charged complexes were performed with $[N^{(t)Bu}_4][B(C_6F_5)_4]$ and $[N^{(t)Bu}_4][B(C_6H_3(CF_3)_2)_4]$ as supporting electrolyte. The wide range of twelve reduction processes was best resolved in THF.

The ferrocenyl group of β -diketone **4** exhibited reversible electrochemistry in CH_3CN as well as in CH_2Cl_2 . The ruthenocenyl fragment exhibited irreversible electrochemistry in $CH_3CN/[N^{(t)Bu}_4][PF_6]$. Results were consistent with formation of the Ru^{IV} species $[(C_5H_4R)(Cp)Ru^{IV}(CH_3CN)]^{2+}$. In $CH_2Cl_2/[N^{(t)Bu}_4][B(C_6F_5)_4]$, however, clear evidence for the electrochemically reversible generation of $[(C_5H_5)Ru^{III}(C_5H_4R)]^+$ in chemical equilibrium with a

dimerised oxidised product, including $[(C_5H_4R)(C_5H_5)Ru^{III}-Ru^{III}(C_5H_5)(C_5H_4R)]^{2+}$, was found.

Acknowledgement

The authors acknowledge the UFS for financial support and Dr. I. Chambrier for supplying samples of **3**.

Appendix A. Supplementary material

Supplementary data associated with this article can be found, in the online version, at doi:10.1016/j.ica.2010.03.031.

References

- (a) D.H. Evans, K.M. O'Connell, R.A. Peterson, M.J. Kelly, J. Chem. Educ. 60 (1983) 291;
- (b) P.T. Kissinger, W.R. Heineman, J. Chem. Educ. 60 (1983) 702;
- (c) J.J. Van Benschoten, J.Y. Lewis, W.R. Heineman, J. Chem. Educ. 60 (1983) 772;
- (d) G.A. Mobbott, J. Chem. Educ. 60 (1983) 697.
- (2) M. Lovric, in: F. Scholz (Ed.), *Electroanalytical Methods: Guide to Experiments and Applications*, Springer, Berlin, 2005 (Chapter I.2, p. 23 and Chapter II.3, pp. 111–133).
- (3) (a) D.E. Richardson, H. Taube, Inorg. Chem. 20 (1981) 1287;
- (b) A. Auger, J.C. Swarts, Organometallics 26 (2007) 102;
- (c) A. Auger, A.J. Muller, J.C. Swarts, Dalton Trans. (2007) 3623.
- (4) M. Schnippering, A. Zahn, S.-X. Liu, C. Leumann, S. Decurtins, D.J. Fermin, Chem. Commun. (2009) 5552.
- (5) E. Fourie, J.C. Swarts, D. Lorcy, N. Bellec, Inorg. Chem. 49 (2010) 952.
- (6) D.G. Leait, Electrochim. Acta 36 (1991) 309.
- (7) J. Conradie, T.S. Cameron, M.A.S. Aquino, G.J. Lamprecht, J.C. Swarts, Inorg. Chim. Acta 358 (2005) 2530.
- (8) Leading publications demonstrating the influence and use of $[B(C_6F_5)_4]^-$ and $[B(C_6H_3)(CF_3)_2]_4^-$ ions, the complimentary role of associated cations with different charge densities, as well as some solvent effects may be found in (a) F. Barriere, R.U. Kirss, W.E. Geiger, Organometallics 24 (2005) 48. and references therein;
- (b) S. Trupia, A. Nafady, W.E. Geiger, Inorg. Chem. 42 (2003) 5480;
- (c) F. Barriere, N. Camire, W.E. Geiger, U.T. Mueller-Westerhoff, R. Sanders, J. Am. Chem. Soc. 124 (2002) 7262;
- (d) F. Barriere, W.E. Geiger, J. Am. Chem. Soc. 128 (2006) 3980;
- (e) A. Nafady, T.T. Chin, W.E. Geiger, Organometallics 25 (2006) 1654;
- (f) D.S. Chong, J. Slote, W.E. Geiger, J. Electroanal. Chem. 630 (2009) 28;
- (g) M.G. Hill, W.M. Lamanna, K.R. Mann, Inorg. Chem. 30 (1991) 4687.
- (9) G. Gritzner, J. Kuta, Pure Appl. Chem. 56 (1984) 461.
- (10) R.R. Gagne, C.A. Koval, G.C. Lisensky, Inorg. Chem. 19 (1980) 2855.
- (11) Leading references describing the electrochemical activity and behaviour of ferrocene and decamethylferrocene in a multitude of organic solvents is (a) I. Noviadri, K.N. Brown, D.S. Fleming, P.T. Gulyas, P.A. Lay, A.F. Masters, L. Phillips, J. Phys. Chem. B 103 (1999) 6713;
- (b) N.G. Connelly, W.E. Geiger, Chem. Rev. 96 (1996) 877.
- (12) (a) C.E.J. Van Rensburg, E. Kreft, J.C. Swarts, S.R. Dalrymple, D.M. Macdonald, M.W. Cooke, M.A.S. Aquino, Anticancer Res. 22 (2002) 889;
- (b) M.W. Cooke, C.A. Murphy, S.T. Cameron, J.C. Swarts, M.A.S. Aquino, Inorg. Chem. Comm. 3 (2000) 721;
- (c) M.W. Cooke, T.S. Cameron, K.N. Robertson, J.C. Swarts, M.A.S. Aquino, Organometallics 21 (2002) 5962.
- (13) M.J. Cook, I. Chambrier, G. White, E. Fourie, J.C. Swarts, Dalton Trans. (2009) 1136.
- (14) K.C. Kemp, E. Fourie, J. Conradie, J.C. Swarts, Organometallics 27 (2008) 357.
- (15) (a) I. Chambrier, D.L. Hughes, J.C. Swarts, B. Isare, M.J. Cook, Chem. Commun. 3504 (2006);
- (b) I. Chambrier, G. White, M.J. Cook, Chem. Eur. J. 13 (2007) 7608.
- (16) R.J. Lesuer, C. Buttolph, W.E. Geiger, Anal. Chem. 76 (2004) 6395.
- (17) (a) C. Creutz, H.J. Taube, J. Am. Chem. Soc. 91 (1969) 3988;
- (b) W.E. Geiger, N. Van Order, D.T. Pierce, T.E. Bitterwolf, A.L. Reingold, N.D. Chasteen, Organometallics 10 (1991) 2403;
- (c) N. Van Order, W.E. Geiger, T.E. Bitterwolf, A.L. Reingold, J. Am. Chem. Soc. 109 (1987) 5680;
- (d) D.T. Pierce, W.E. Geiger, Inorg. Chem. 33 (1994) 373;
- (e) W.L. Davis, R.F. Shago, E.H.G. Langner, J.C. Swarts, Polyhedron 24 (2005) 1611;
- (f) W.C. Du Plessis, J.J.C. Erasmus, G.J. Lamprecht, J. Conradie, T.S. Cameron, M.A.S. Aquino, J.C. Swarts, Can. J. Chem. 77 (1999) 378;
- (g) J. March, *Advanced Organic Chemistry*, fourth ed., John Wiley and Sons, New York, 1992, pp. 17–20, 263–269, 273–275.
- (18) (a) J.C. Swarts, E.H.G. Langner, N. Krokeide-Hove, M.J. Cook, J. Mater. Chem. 11 (2001) 434;
- (b) E. Fourie, J.C. Swarts, I. Chambrier, M.J. Cook, Dalton Trans. (2009) 1145;
- (c) M. L'Her, A. Pondaven, in: K.M. Kadish, R. Guillard, K.M. Smith (Eds.), *The*

- Porphyrin Handbook, vol. 16, Academic Press, Elsevier Science, USA, pp. 117–169.
- [19] T. Kuwana, D.E. Bublitz, G. Hoh, J. Am. Chem. Soc. 82 (1960) 5811.
- [20] (a) M. Watanaba, I. Motoyama, T. Takayama, M. Sato, J. Organomet. Chem. 549 (1997) 13;
(b) M. Watanaba, I. Motoyama, M. Shimoi, H. Sano, J. Organomet. Chem. 517 (1996) 115;
(c) T.P. Smith, D.J. Iverson, M.W. Droege, K.S. Kwan, H. Taube, Inorg. Chem. 26 (1987) 2882.
- [21] J.C. Swarts, A. Nafady, J.H. Roudebush, S. Trupia, W.E. Geiger, Inorg. Chem. 48 (2009) 2156.
- [22] M.W. Droege, W.D. Harman, H. Taube, Inorg. Chem. 26 (1987) 1309.